ChemComm

COMMUNICATION

View Article Online
View Journal | View Issue

Cite this: *Chem. Commun.*, 2021, **57**, 13740

Received 22nd October 2021,
Accepted 19th November 2021

DOI: 10.1039/d1cc05960b

rsc.li/chemcomm

Ultrasound-assisted dopamine polymerization: rapid and oxidizing agent-free polydopamine coatings on membrane surfaces†

Aydın Cihanoğlu,[a] Jessica D. Schiffman [b] and Sacide Alsoy Altinkaya *[a]

Herein, we report a controllable pathway to accelerate the polymerization kinetics of dopamine using ultrasound as a trigger. The use of ultrasound was demonstrated to dramatically accelerate the slow liquid phase reaction kinetics and increase the deposition rate of the polydopamine coating on the surface of polymeric membranes.

Surface modification with mussel-inspired dopamine coatings have attracted great interest due to the presence of catechol (DOPA) and amine (lysine) groups that form strong covalent and noncovalent interactions with a broad spectrum of organic and inorganic materials, such as polymers, metals, and ceramics.[1,2] Additionally, established polydopamine (PDA) coatings can easily be post-modified by various molecules, including thiols,[1] and amines,[3] owing to the presence of functional groups in the PDA structure. Due to their high negative charge density and hydrophilicity, PDA coatings have also been explored for many membrane applications, such as wastewater treatment,[4] battery separators,[5] nanofiltration[6] and gas separation.[7] In all of these applications, superior performance of the membrane, such as high-water flux,[6] excellent water vapor/N_2 selectivity,[7] and high fouling resistance[8] was directly, or indirectly related to the PDA layer. Despite the unique properties of PDA coatings, the slow kinetics of dopamine polymerization, which range from several hours to a few days, remains an issue.[9–13] Thus, the PDA coatings process is too time-consuming and restricts their large-scale industrial applications. Different strategies utilizing UV,[10] microwave,[9] microplasma,[11] and chemical oxidizing agents[12,13] have accelerated the polymerization rate to overcome this drawback. However, these techniques have their own limitations, such as degradation of the membrane support due to UV irradiation,[14] surface contamination of the triggering metal ions,[13] the need for chemical oxidizing agents,[12] and high energy requirements which can increase the temperature to 100 °C within a few minutes.[9] The high temperature during polymerization can lead to collapsed pores in the support membrane.

In polymer science, ultrasound has been used to degrade synthetic and bio-based polymers for nearly half a century,[15] control aggregation during the coating of inorganic nanoparticles,[16] and applied to various polymer synthesis techniques, such as sono-chemically induced reversible addition fragmentation chain transfer polymerization (Sono-RAFT)[17] and sonochemically induced nitroxide-mediated polymerization (Sono-NMP).[18] However, ultrasound has never been utilized for surface modification of membranes, which is what we demonstrate in this work.

In this study, we establish for the first time that ultrasound can be used as a trigger to significantly accelerate the polymerization kinetics of dopamine in the liquid phase, and the deposition rate of a PDA film on porous polymeric membranes at room temperature without using any chemical oxidizing agents. PDA coatings were successfully formed on hydrophobic polysulfone (PSF) and relatively hydrophilic, polysulfone-sulfonated polyethersulfone (PSF-SPES) membranes that are commonly used in separation applications. The effect of the ultrasound triggering on the PDA coating was evaluated using surface free energy (SFE), contact angle, XPS, SEM, AFM, ATR-FTIR, pure water permeability (PWP) and polyethylene glycol (PEG) rejection measurements. In addition, the high-performance of the PDA-coated membranes was demonstrated *via* antifouling experiments using oil/water emulsions as a foulant. The impact of ultrasound on the structure of the bare membranes was investigated through PWP and PEG rejection experiments before and after ultrasound exposure. This study provides a rapid polymerization and also opens a new direction for the applications of ultrasound-assisted based polymerization of dopamine.

First, we explored the qualitative colour change and quantified UV/Vis absorbance of the dopamine solution (2 mg mL^{-1}, 10 mM Tris-HCl, pH = 8.5) as a function of reaction time with and without sonification, as shown in Fig. 1. The colour of the solution turned a characteristic darker brown within 15 min in ultrasound-assisted polymerization (USP), while very little colour change was observed even after 60 min in conventional

[a] *Faculty of Engineering, İzmir Institute of Technology, department of Chemical Engineering, Urla, İzmir, 35430, Turkey. E-mail: sacidealsoy@iyte.edu.tr*
[b] *University of Massachusetts-Amherst, Department of Chemical Engineering, Massachusetts, 01003, USA*

† Electronic supplementary information (ESI) available. See DOI: 10.1039/d1cc05960b

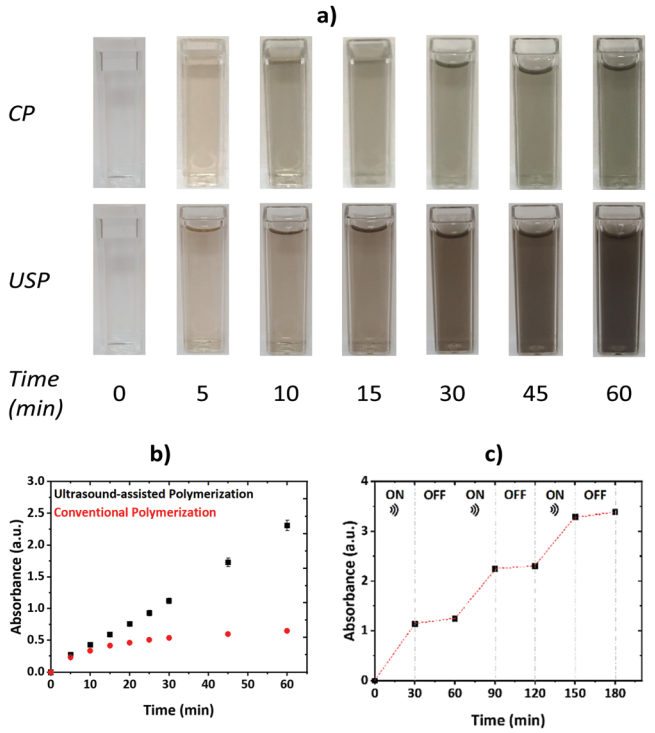

Fig. 1 (a) Color change of the dopamine solution as a function of time. (b) Time-dependence of absorbance at 420 nm. (c) Absorbance changes by turning ON and OFF of the ultrasound.

polymerization (CP) (Fig. 1a). When using the USP technique, the absorbance of the characteristic peak at 420 nm, attributed to the PDA, increased from 0 to 2.31 ± 0.16 after 60 min, which was much higher than the value observed using CP as shown in Fig. 1b. To demonstrate the effectiveness and controllability of the ultrasound system, the solution was exposed to the USP for 30 min (ON) and then to the CP for 30 min (OFF), and this cycle was repeated three times. The result in Fig. 1c shows that the absorbance intensity of the PDA increased sharply when the ultrasound was applied. On the contrary, the change was insignificant during the CP, which demonstrates that the ultrasound accelerated the polymerization kinetics of dopamine in liquid phase.

Fig. S1a (ESI†) shows that the rate of dopamine polymerization was higher at a low ultrasound frequency (20 kHz, 30 W). At high frequency (850 kHz, 25 W), the amount of intermediate product, H_2O_2,[19] increased considerably which suppressed the polymerization kinetics by degrading the PDA formed.[13,20] Based on the results in Fig. S1a (ESI†), low-frequency (20 kHz) ultrasound was applied for further investigations. We hypothesize that the ultrasound accelerates the dopamine polymerization through enhanced reactive oxygen species (ROSs) formation by decomposition of water molecules.[15] To prove this hypothesis, a nitroblue tetrazolium (NBT) assay was used in the liquid phase polymerization by adding 0.82 mg mL^{-1} NBT into dopamine solution. NBT reacts with ROSs and forms a light absorbing molecule (at 560 nm), blue NBT formazan.[21,22] The absorbance reading at 560 nm is a direct measure of the ROSs level in the solution.[9] Thus, according to the results in Fig. S1b (ESI†), higher absorbance values measured during USP proved enhanced ROSs generation with ultrasound triggering. Dopamine polymerization was inhibited by the addition of radical scavengers, ascorbic acid (2 mg mL^{-1}) and cysteine (2 mg mL^{-1}) (Fig. S2, ESI,† EDI). The pH value of the solution was adjusted to 8.5 after adding the radical scavengers. The inhibition was due to quenching the generated radicals[23,24] and not due to pH change in the solution.[25] This result confirmed that the radical generation is the key mechanism for the dopamine polymerization.

In literature, the rate of dopamine deposition is generally quantified using spectroscopic ellipsometry.[9–13] However, this technique is limited to inorganic samples with smooth surfaces and cannot be applied to the polymeric membranes prepared by phase inversion. To compare the PDA deposition rates by CP and USP techniques, we characterized the coatings using ATR-FTIR spectroscopy, contact angle, surface free energy and XPS measurements. In addition, the changes in surface morphology of the membranes after coating were characterized by AFM and SEM analysis. In the spectrum of the PDA coated membranes, three IR band intensities belonging to the ν(N–H) and ν(O–H) peaks at 3300 cm^{-1} and vring(C═C) peaks at 1623 cm^{-1} were observed, which indicated the presence of dopamine on the membrane surfaces (Fig. S3, ESI†). The area under the ν(N–H) and ν(O–H) peaks was found larger in the case of USP which demonstrated that the kinetics of PDA deposition process was accelerated using ultrasound as a trigger (Table S1, ESI†).

Table S2 (ESI†) provides the water contact angles of the bare and PDA coated membranes. The hydrophilicity of both membranes increased upon PDA coating as a result of hydrophilic groups such as –OH, –COOH and $–NH_2$ in the PDA layer. On the other hand, a more hydrophilic surface was obtained on both supports by USP. The SFE of the PDA coated membranes are summarized in Table S3 (ESI†) and compared with those determined for the uncoated membranes (Table S4, ESI†). The PDA coating obtained in the presence of an ultrasonic horn resulted in a larger increase in the SFE's of both membranes. Mostly, the polar component (σ_s^p) of the SFE increased since the PDA has polar functional groups, such as OH and NH.[26] The increase in the polar component was more pronounced when the PDA was deposited on the hydrophobic PSF support. XPS analysis quantitatively determined the chemical composition of the unmodified and PDA modified membranes. The general survey shows that unmodified membranes possessed characteristic peaks of C1s, O1s, S2s and S2p, while the modified ones have an additional N1s peak (Fig. S4, ESI†). Sulfur comes from the PSF and SPES. The nitrogen peak that was detected only in the modified membranes confirmed the presence of the PDA layer on both supports. To illustrate the effect of ultrasound on the PDA deposition rates, we considered the N/S ratios of the membranes coated by two techniques. Compared with the CP technique, the PDA coating in the presence of ultrasound resulted in larger N/S ratio (Table S5, ESI†).

AFM images and surface roughness of the PSF and PSF-SPES membranes are provided in Fig. S5 and Table S6 (ESI†),

respectively. The PDA coating on both membranes increased their surface roughness. However, the membranes coated in the presence of ultrasound had lower roughness values. Ultrasound creates a vibration that prevents aggregate formation on the membrane surfaces during coating, thus, enabling to produce smoother surfaces. When the PDA was coated on the PSF-SPES membrane, the effect of ultrasound was more prominent as the roughness of this membrane is significantly lower compared to its counterpart prepared with CP. The surface morphology of the PSF membranes did not change significantly after coating with the PDA layer as shown in Fig. S6 (ESI†). However, PDA aggregates were observed on the PSF-SPES membrane coated with CP without ultrasound.

Recent studies have shown that PDA coatings on different surfaces exhibit strong stability in acidic, neutral, and weak alkaline solutions, but disintegrate in a strongly alkaline condition.[13,27,28] We also observed a similar behavior for the PDA coated PSF-SPES membranes. The absorbance measured at 420 nm in NaOH solution was higher for the PSF-SPES membrane coated with CP, which corresponds to more PDA leaching from the surface after 24 hours (Fig. S7, ESI†). This result demonstrated that the USP had a positive impact on the stability of the PDA coating. The lower stability of the PDA layer on the PSF-SPES membrane formed with CP could be due to the deposition of PDA as aggregates (Fig. S6, ESI†). In addition, the ultrasound may have changed the mechanism of PDA deposition which is still not clear in literature.[29] Nevertheless, further studies are needed to investigate the effect of ultrasound on the deposition mechanism and the binding strength of the PDA layer. The thermal stability was not evaluated since filtration with polymeric membranes is mostly carried out at room temperature. The coating was very stable at room temperature.

Changes to the membrane structure after ultrasound treatment were established by measuring if the rejection and permeability values changed. Fig. 2 shows that the PWP and PEO 100 kDa (polyethylene oxide) rejection values of the uncoated membranes before and after 1 hour ultrasound exposure remained constant. This promising result demonstrates that the ultrasound did not cause any change in the structure of the support membranes and contrasts previous results observed when UV irradiation was used. For example, Baek *et al.*[14] used UV irradiation to shorten the PDA coating time on polyamide reverse osmosis membrane. However, 30 min UV irradiation caused an increase in NaCl rejection from 1% to 3%, which indicated the degradation of the polyamide membrane. Similarly, Rupiasih *et al.*[30] reported the adverse effect of a very short time (2 min) UV irradiation on the performance of PSF membranes. In this respect, UV irradiation does not seem to be a suitable technique for speeding up the PDA coating.

PDA coatings result in a reduction in membrane's pores, hence, causes decrease in PWP and the increase in the rejection (35 kDa PEG) as presented in Fig. 3. The changes are directly proportional to the amount of PDA deposition, therefore, higher changes in the PWP and rejection values of the membranes coated with USP serves as additional evidence of enhanced polymerization by ultrasound triggering. Both techniques had a larger influence on the PSF membrane due to its smaller pore size which was also reported by McCloskey *et al.*[8] As shown in Table S7 (ESI†), the PDA hydraulic resistance on the PSF membrane was significantly higher than the coated PSF-SPES's resistances. Ultrasound more effectively coated the PSF-SPES membranes; the permeability of this membrane decreased by 21.4% and 63.6% when coated with CP and USP techniques. On the other hand, the difference in the PWP of the PSF membranes modified with the two techniques was smaller. This result is in agreement with the, contact angle, FTIR-ATR SFE and XPS analysis results in Tables S1–S3 and S5 (ESI†).

The antifouling behavior of the bare and PDA coated membranes was evaluated by conducting dynamic filtration experiments using water/paraffin emulsions. The initial water flux of the membranes was adjusted to a similar value by controlling transmembrane pressure difference (TMP). As shown in Fig. 4, at the beginning of filtration, the flux decreased sharply due to the accumulation of large oil particles on the membrane surface, consistent with the literature.[31,32] Flux decline through the PSF-SPES membranes was higher than the PSF membrane due to their larger pore sizes. The PDA coating improved the antifouling properties of the both membranes by ~30%. The membranes coated with USP technique showed lower flux reduction than their counterparts modified with CP. This observation is directly related with more PDA deposition by the use of an ultrasound leading to a more hydrophilic surface (Table S2, ESI†). The surface roughness of the membranes did not play a role on the fouling tendencies since the size of oil droplets (Fig. S8, ESI†) is significantly larger than the roughness of the membranes. Ultrasound triggering increased the flux recovery ratio (FRR) of the coated PSF-SPES membrane with CP from 51.7% to 59.3%. The difference in the FRR of the PSF membranes coated with and without ultrasound was smaller.

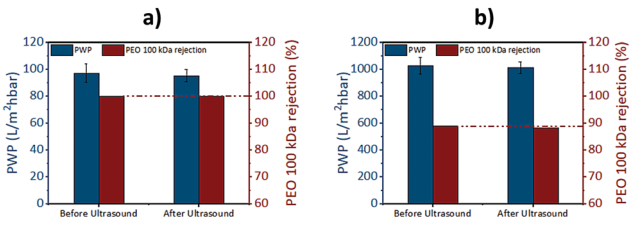

Fig. 2 Effect of ultrasound on PWP and PEO 100 kDa rejection values of unmodified (a) PSF, (b) PSF-SPES membranes before and after 1 hour ultrasound exposure.

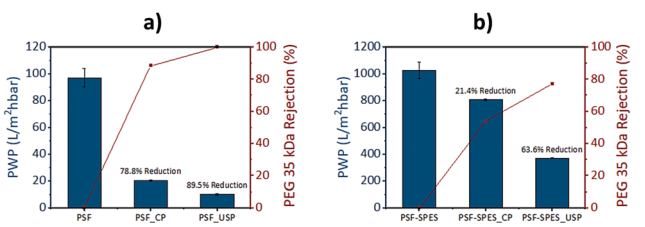

Fig. 3 The PWP and PEG 35 kDa rejection of the unmodified and PDA modified (a) PSF, (b) PSF-SPES membranes.

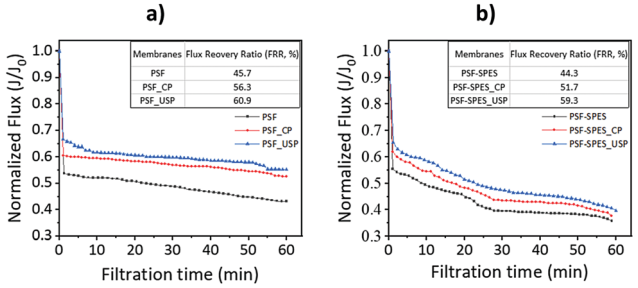

Fig. 4 Normalized flux of (a) PSF, PSF_CP, and PSF_USP, (b) PSF-SPES, PSF-SPES_CP, and PSF-SPES_USP membranes as a function of time during water/paraffin emulsion filtration. Initial water fluxes of PSF, PSF_CP, and PSF_USP membranes were 19.5 ± 1.4, 20.6 ± 0.5 and 20.4 ± 0.6 L m^{-2} h^{-1}, respectively. Initial water fluxes of PSF-SPES, PSF-SPES_CP, and PSF-SPES_USP membranes were 410.4 ± 24.8, 403.4 ± 5.1 and 410.4 ± 4.2 L m^{-2} h^{-1}, respectively.

The filtration results once more confirmed that the ultrasound was more effective on the coating of the PSF-SPES membrane.

In conclusion, we report for the first time that the slow kinetics of dopamine polymerization on polymeric membrane surfaces can be accelerated by ultrasound triggering. The liquid phase polymerization studies proved that the acceleration occurs due to enhanced ROSs formation through the decomposition of water molecules. All of the surface characterization results, and oily water filtration studies demonstrate that the kinetics of PDA coating on both membranes was enhanced. Notably, ultrasound had a more prominent effect on the PSF-SPES supports due to their higher hydrophilicity, which likely lead to more contact between the dopamine solution and the membrane surface during the polymerization. The structures of the bare membranes were not affected by the ultrasound exposure. The PDA deposition improved oil/water fouling resistance of the membranes. However, the membranes modified with ultrasound had higher fouling resistance and chemical stability than their counterparts coated without ultrasound. USP avoids chemical oxidizing agents and can be applied at room temperature on various polymeric membranes without changing the bulk structures. Most importantly, the method can be applied at large industrial scales which makes it convenient for the modification of large membrane areas. We anticipate that an environmentally friendly USP could enhance the efficiency of the PDA coating on membranes for large scale applications by shortening the coating time. There may be a trade-off between energy used to produce the coating and the shorter coating time but doing those calculations on an industrial scale is beyond our capabilities.

One of the authors, Aydın Cihanoğlu, was supported by the Scientific and Technological Research Council of Turkey (TÜBİTAK) with (2211/E) National PhD Scholarship program. J. D. S. acknowledges the support from the National Science Foundation (award 1930610). We would like to thank the Material Research Center and Biotechnology and Bioengineering Application Research Center at the İzmir Institute of Technology for their kind help and technical support. Also thanks to, Professor Gönül Gündüz, Professor Funda Tihminlioglu, Assoc. Professor Sevgi Kılıç and Assoc. Professor Meral Dükkancı for providing ultrasound equipments.

Conflicts of interest

There are no conflicts to declare.

Notes and references

1 H. Lee, S. M. Dellatore, W. M. Miller and P. B. Messersmith, *Science*, 2007, **318**, 426–430.
2 H. Lee, N. F. Scherer and P. B. Messersmith, *Proc. Natl. Acad. Sci. U. S. A.*, 2006, **103**, 12999.
3 S. M. Kang, N. S. Hwang, J. Yeom, S. Y. Park, P. B. Messersmith, I. S. Choi, R. Langer, D. G. Anderson and H. Lee, *Adv. Funct. Mater.*, 2012, **22**, 2949–2955.
4 S. Kasemset, A. Lee, D. J. Miller, B. D. Freeman and M. M. Sharma, *J. Membr. Sci.*, 2013, **208**, 425–426.
5 M. H. Ryou, D. J. Lee, J. N. Lee, Y. M. Lee, J. K. Park and J. W. Choi, *Adv. Energy Mater.*, 2012, **2**, 645.
6 Y. Li, Y. Su, J. Li, X. Zhao, R. Zhang, X. Fan, J. Zhu, Y. Ma, Y. Liu and Z. Jiang, *J. Membr. Sci.*, 2015, **476**, 10.
7 P. G. Ingole, W. K. Choi, I.-H. Baek and H. K. Lee, *RSC Adv.*, 2015, **5**, 78950.
8 B. D. McCloskey, H. B. Park, H. Ju, B. W. Rowe, D. J. Miller and B. D. Freeman, *J. Membr. Sci.*, 2012, **413**, 82–90.
9 M. Lee, S. H. Lee, I. K. Oh and H. Lee, *Small*, 2017, **13**, 1600443.
10 X. Du, L. Li, J. Li, C. Yang, N. Frenkel, A. Welle, S. Heissler, A. Nefedov, M. Grunze and P. A. Levkin, *Adv. Mater.*, 2014, **26**, 8029–8033.
11 Z. Wang, C. Xu, Y. Lu, G. Wei, G. Ye, T. Sun and J. Chen, *Polym. Chem.*, 2017, **8**, 4388–4392.
12 J. Wang, G. Ma, W. Huang and Y. He, *Polym. Chem.*, 2018, **9**, 5242–5247.
13 C. Zhang, Y. Ou, W. X. Lei, L. S. Wan, J. Ji and Z. K. Xu, *Angew. Chem., Int. Ed.*, 2016, **55**, 3054–3057.
14 Y. Baek, B. D. Freeman, A. L. Zydney and J. Yoon, *Ind. Eng. Chem. Res.*, 2017, **56**, 5756–5760.
15 J. M. J. Paulusse and R. P. Sijbesma, *J. Polym. Sci., Part A: Polym. Chem.*, 2006, **44**, 5445–5453.
16 D. G. Meeker, S. V. Jenkins, E. K. Miller, K. E. Beenken, A. J. Loughran, A. Powless, T. J. Muldoon, E. I. Galanzha, V. P. Zharov, M. S. Smeltzer and J. Chen, *ACS Infect. Dis.*, 2016, **2**, 241–250.
17 J. Collins, T. G. McKenzie, M. D. Nothling, S. Allison-Logan, M. Ashokkumar and G. G. Qiao, *Macromolecules*, 2019, **52**, 185–195.
18 T. G. McKenzie, E. Colombo, Q. Fu, M. Ashokkumar and G. G. Qiao, *Angew. Chem., Int. Ed.*, 2017, **56**, 12302–12306.
19 T. G. McKenzie, F. Karimi, M. Ashokkumar and G. G. Qiao, *Chem. – Eur. J.*, 2019, **25**, 1–18.
20 Z. Wang, K. Wang, Y. Zhang, Y. Jiang, X. Lu, L. Fang, D. Gan, C. Lv, H. Zhang and S. Qu, *Part. Part. Syst. Charact.*, 2016, **33**, 89.
21 C. Auclair, M. Torres and J. Hakim, *FEBS Lett.*, 1978, **89**, 26–28.
22 M. Matsuoka, F. Takahashi, Y. Asakura and J. Jin, *Jpn. J. Appl. Phys.*, 2016, **55**, 07KB01.
23 E. Niki, *Am. J. Clin. Nutr.*, 1991, **54**, 1119–1124.
24 T. C. P. Dinis, V. M. C. Madeira and L. M. Almeida, *Arch. Biochem. Biophys.*, 1994, **315**, 161–169.
25 X. Du, L. Li, F. B. Sadabad, A. Welle, J. Li, S. Heissler, H. Zhang, N. Plumere and P. A. Levkin, *Polym. Chem.*, 2017, **8**, 2145.
26 J. Jiang, L. Zhu, L. Zhu, B. Zhu and Y. Xu, *Langmuir*, 2011, **27**, 14180–14187.
27 L. Yao, C. He, S. Chen, W. Zhao, Y. Xie, S. Sun, S. Nie and C. Zhao, *Langmuir*, 2019, **35**, 1430–1439.
28 C. C. Chang, K. W. Kolewe, Y. Li, I. Kosif, B. D. Freeman, K. R. Carter, J. D. Schiffman and T. Emrick, *Adv. Mater. Interfaces*, 2016, **3**, 1500521.
29 D. R. Dreyer, D. J. Miller, B. D. Freeman, D. R. Paul and C. W. Bielawski, *Chem. Sci.*, 2013, **4**, 3796–3802.
30 N. N. Rupiasih, H. Suyanto, M. Sumadiyasa and N. Wendri, *Open J. Org. Polym. Mater.*, 2013, **3**, 12–18.
31 Z. He, D. J. Miller, S. Kasemset, D. R. Paul and B. D. Freeman, *J. Membr. Sci.*, 2017, **525**, 25–34.
32 Z. He, D. J. Miller, S. Kasemset, L. Wang, D. R. Paul and B. D. Freeman, *J. Membr. Sci.*, 2016, **514**, 659–670.

Ultrasound-assisted dopamine polymerization: rapid and oxidizing agent-free polydopamine coatings on membrane surfaces

Aydın Cihanoğlu,[a] Jessica D. Schiffman [b] and Sacide Alsoy Altınkaya*[a]

[a] İzmir Institute of Technology, Faculty of Engineering, Department of Chemical Engineering, 35430, Urla, İzmir, TURKEY

[b] University of Massachusetts-Amherst, Department of Chemical Engineering, Massachusetts, 01003, USA

***Corresponding author (E-mail: sacidealsoy@iyte.edu.tr)**

Table of Contents

Materials

Dopamine hydrochloride, Tris-HCl buffer, $_{L}$-ascorbic acid, Cysteine, nitrotetrazolium blue chloride (NBT) were purchased from Sigma-Aldrich. Polysulfone (PSF) (Mw= 35 kDa) purchased from Sigma-Aldrich, and Sulfonated polyethersulfone (SPES) (Mw= 80 kDa, Sulfonation degree (SD)<30%) kindly donated by Konishi Chemicals, Japan, were used to prepare flat sheet membranes. 1-methyl-2-pyrrolidone (NMP, 99.5%) and N, N-Dimethylacetamide (DMAc, 99%) purchased from Fluka and Sigma-Aldrich, were used to dissolve the polymers. NaOH, HCl, polyethylene glycol (PEG: 35 kDa) and polyethylene oxide (PEO: 100 kDa) were purchased from Sigma-Aldrich. The water/paraffin emulsion used to determine the fouling resistance of the membranes was kindly supplied by Işıksan Kimya Corporation and Polyester non-woven fabric (05TH-100) (thickness: 161 µm and base weight: 100 g/m^2) was purchased from Hirose Paper Mfg. Co. Ltd, Japan, and used as a support layer for manufacturing the membranes. All chemicals were used without further purification and solutions were prepared using deionized (18.2 MΩ cm) water.

Preparation of Flat Sheet Membranes

PSF and PSF-SPES blend membranes were prepared by the non-solvent induced phase inversion technique. The polymers were dried in a vacuum oven at 80 ^{o}C for 24 h to remove moisture. Dried PSF and the PSF:SPES blend (blending ratio is 3:1) were dissolved in NMP and DMAc:NMP mixture (DMAc:NMP ratio of 2:1), respectively by stirring at 100 rpm for 24 h. In order to eliminate air bubbles, solutions rested for 24 h without stirring and then were cast on a clean glass plate and non-woven with the help of an automated film applicator (Sheen Instrument Ltd., model number: 1133N). The initial thickness of the cast membranes was adjusted using a four-sided applicator with a gap size of 200 µm. Following casting, the glass plate was immediately immersed into the coagulation bath including only deionized (18.2 MΩ cm) water at 25 ^{o}C. The polymer concentration in both casting solutions was adjusted to 20 wt.%.

Conventional and Ultrasound-Assisted Polymerization of Dopamine

Dopamine hydrochloride (2 mg/mL) was dissolved in Tris-HCl buffer solution (10 mM, pH 8.5, 25 ^{o}C). For conventional polymerization (Scheme 1a), the reaction solution (100 mL) was gently shaken at 70 rpm and room (25 ^{o}C) temperature. For ultrasound-assisted polymerization, an ultrasonic horn (Scheme 1b) and an ultrasonic reactor (Scheme 1c) operated at 30 W (frequency 20 kHz) and 25 W were used. In both experimental setup, the dopamine solution (100 mL) was not stirred, and the temperature was controlled by a chiller. At specific time intervals, the sample was removed to measure the formed polydopamine intensity using UV-vis spectroscopy. For coating the membranes, the sample coupons were immersed in the dopamine solution for 1 h under the same conditions used for bulk polymerization.

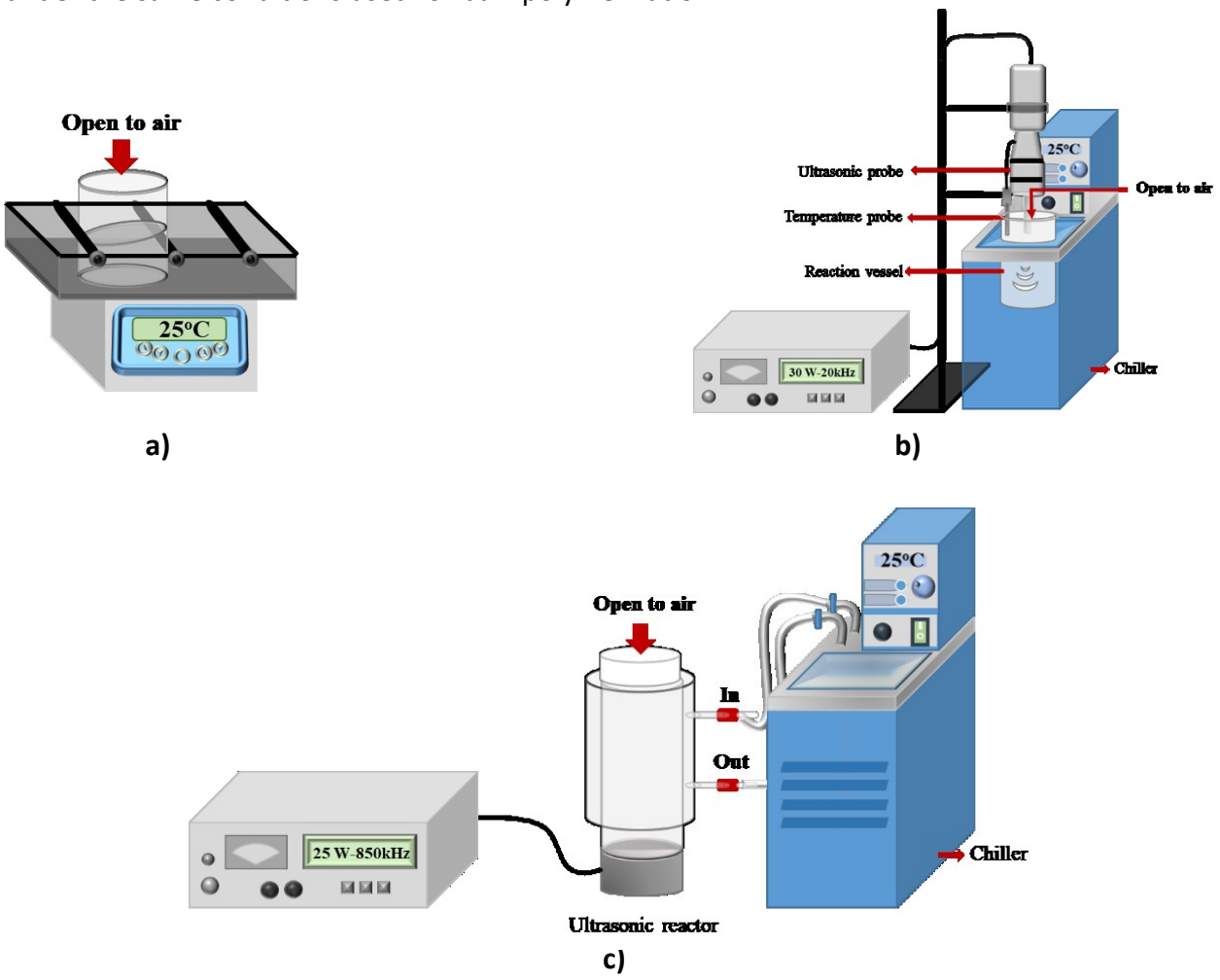

Scheme 1 a) Conventional polymerization set-up, **b)** Ultrasonic horn polymerization set-up **c)** Ultrasonic reactor polymerization set-up

Characterization of Membranes

The chemical structure of the bare and modified membranes was determined by Attenuated Total Reflectance Fourier Transformed Infrared Spectrometer (ATR-FTIR), (Perkin Elmer). Spectra were collected at ambient temperature over a scanning range of 4000-650 cm^{-1} with a resolution of 4.0 cm^{-1}. The water contact angle of the membranes was measured (Attension Optical tensiometer) with a 5 µL water droplet (*n*=5). The surface free energy (SFE) calculations based on the OWRK method (Owens, Wendt, Rabel and Kaelble) were carried out using the contact angle measurements of water and diiodomethane. The X-ray photoelectron spectra (XPS, Thermo Scientific) analysis at the emission angle of 0° was used to determine the elemental composition of the membranes (*n*=3). The surface morphology of the membranes was characterized using a scanning electron microscope (SEM) (FEI Quanta 250 FEG). Before taking the images, the membrane surfaces were coated with gold nanoparticles with a Magnetron Sputter Coating Instrument. The surface roughness of the membranes (arithmetic mean (R_a) and root-mean-square (R_q)) was determined using an atomic force microscope (AFM) (MMSPM Nanoscope 8, Bruker). 5 × 5 μm^2 sample area was scanned at a rate of 1 Hz using tapping mode in the air at room temperature by the TAP150 model tip (Bruker) (*n*=3). Prior to analysis, all the membranes were dried in a vacuum oven (Memmert) at 25 °C. (*n* is the number of repeated experiments).

The surface free energy (SFE) values were determined by the OWRK method.[1] Equation 1 describes the surface tension of the solid (σ_s) with respect to the interfacial tension between solid and liquid (σ_{sl}) and the surface tension of the liquid (σ_l) by the Young equation:

$$\sigma_s = \sigma_{sl} + \sigma_l . cos\theta \quad (1)$$

The OWRK method requires contact angle measurements with at least two liquids, one polar (water) and the other nonpolar (diiodomethane) to calculate σ_s and the σ_l from Equation 2.

$$\sigma_l = \sigma_l^d + \sigma_l^p, \qquad \sigma_s = \sigma_s^d + \sigma_s^p \quad (2)$$

where σ_l^d/σ_s^d and σ_l^p/σ_s^p are the disperse and polar components of the liquid and solid, respectively. The OWRK model uses geometric mean to combine the solid and liquid contributions as follows:

$$\sigma_{sl} = \sigma_s + \sigma_l - 2\left(\sqrt{\sigma_s^d.\sigma_l^d} + \sqrt{\sigma_s^p.\sigma_l^p}\right) \quad (3)$$

Substituting this term for  in the Young equation (1) and solving the unknowns results in a linear expression.

$$y = mx + c \quad (4)$$

where

$$y = \frac{1+cos\theta}{2}\frac{\sigma_l}{\sqrt{\sigma_l^d}}, \qquad x = \sqrt{\frac{\sigma_l^p}{\sigma_l^d}}, \qquad m = \sqrt{\sigma_s^p}, \qquad c = \sqrt{\sigma_s^d} \quad (5)$$

Thus, plotting y versus x enables the calculation of  from the slope, and  from the intersection with the vertical axis.

Membrane Filtration Performance

The filtration performance of membranes was determined by a 50 mL dead-end stirred cell (Millipore, Amicon Stirred Cell 8050) with an effective area of 13.4 cm^2. Before filtration, membrane coupons were compacted until a constant flux is reached. Next, pure water was filtered at 1 bar and collected permeate volume was recorded for specific time intervals. The volumetric flux was calculated from the slope of the permeate volume vs. time graph and converted to hydraulic pure water permeability (PWP) using following equation:

$$PWP = \frac{\Delta V}{A\Delta t\Delta P} \quad (6)$$

where ΔV is the volume of permeated water (L), A (m^2) is the membrane area, Δt (h) is the permeation time and ΔP (bar) is the transmembrane pressure difference applied through the membrane. To determine the rejection characteristics of the membranes, 1 g/L aqueous solutions of 35 kDa PEG and 100 kDa PEO were filtered at 1 bar. The concentrations of the permeate, retentate and feed solutions were measured by Rudolph-J357 Automatic Refractometer. The solute rejection (%) was calculated using the equation:

$$R(\%) = \left(1 - \frac{C_p}{\frac{C_f + C_r}{2}}\right) x100 \quad (7)$$

where C_p, C_r and C_f are the concentrations of permeate, retentate and feed solution, respectively. To eliminate concentration polarization, the solution was stirred at 300 rpm. The fouling behaviour of the membranes was evaluated by filtering of water/paraffin emulsion at 1 bar. Following filtration, the membrane coupons were rinsed with pure water for 30 min and water flux was re-measured to calculate the flux recovery ratio (FRR).

$$FRR(\%) = \left(\frac{J_R}{J_W}\right) x100 \quad (8)$$

where J_W and J_R are the pure water fluxes of the clean and the washed membranes. The experiments were carried out at room (25 ^{o}C) temperature. (n=3 where n is the number of repeated experiments).

The hydraulic resistance of the porous bare and PDA coated membranes is defined as follows:[2]

$$R_i = \frac{\Delta p}{\mu J_i} \quad (9)$$

where Δp is the transmembrane pressure, μ is the viscosity of the feed solution, J_i is the steady-state water flux and R_i is the hydraulic resistance of the membrane.

Equation 9 can be employed for coated membranes to quantify the effect of PDA coating on membrane flux. The coating layer adds resistance to the membrane's overall hydraulic resistance, and it can be expressed as:

$$J_{PDA} = \frac{\Delta p}{\mu(R_0 + R_{PDA})} \quad (10)$$

where J_{PDA} is the pure water flux of PDA coated membrane, R_0 is the hydraulic resistance of bare membrane, R_{PDA} is the hydraulic resistance of the PDA coated membrane. By combining equations 9 and 10, R_{PDA} can be calculated as follows:

$$R_{PDA} = \frac{\Delta p}{\mu}\left(\frac{1}{J_{PDA}} - \frac{1}{J_0}\right) \quad (11)$$

where J_0 is the steady-state pure water flux of bare membrane.

Stability of Coating Layer

The chemical stability of the PDA-coating layer on membranes was evaluated in a strong acidic and alkaline environment. To this end, coated membranes with 1.5 cm x 1.5 cm sizes were immersed in 5 mL 0.1 M NaOH and 0.1 M HCl for 24 h. Next, the leached PDA in solution was quantified by measuring the absorbance of the solution at 420 nm with UV-vis spectroscopy.[3]

Table S1. Peak area of the bare and PDA coated membranes.

Membranes	Peak Area		
	***v*(N-H)** and ***v*(O-H)** peaks at 3300 cm^{-1}		
	Bare	**CP**	**USP**
PSF	41.1	400.5	515.2
PSF-SPES	345.7	2030.1	3918.4

Table S2 Contact angles of the bare and PDA coated membranes.

Membranes	Contact Angle (°)			The change in Contact Angle (%)	
	Bare	CP	USP	$(\theta_B-\theta_{CP})/\theta_B$	$(\theta_B-\theta_{USP})/\theta_B$
PSF	97.4±0.2*	76.9±0.6*	69.9±0.6*	21.0	28.2
PSF-SPES	72.9±0.8**	58.9±0.8**	46.8±0.1**	19.1	35.9

θ_B, θ_{CP}, θ_{USP} are the contact angle of bare, CP, and UPS membranes, respectively.

*represents statistically significant difference ($p<0.05$) in contact angle of the bare and coated PSF membranes.

**represents statistically significant difference ($p<0.05$) in contact angle of the bare and coated PSF-SPES membranes.

Table S3. Surface free energy and its components of the PDA coated membranes.

Membranes	Coating technique	Contact Angle (°)		SFE components (mN/m)			$(\sigma_s^p-\sigma_{so}^p)/\sigma_{so}^p$	$(\sigma_s-\sigma_{so})/\sigma_{so}$
		Water	Diiodomethane	σ_s	σ_s^d	σ_s^p		
PSF	CP	76.9±0.6	32.2±0.4	47.1	43.3	3.8	250.9	0.080
	USP	69.9±0.6	31.7±0.4	49.9	43.5	6.4	427.5	0.146
PSF-SPES	CP	58.9±0.8	29.6±0.3	55.7	44.4	11.3	1.2	0.130
	USP	46.8±0.1	31.3±0.5	61.9	43.7	18.2	2.6	0.255

σ_{so}: The total surface free energies of the modified membranes.

σ_{so}^d and σ_{so}^p: Dispersive and polar components of the surface free energies of the modified membranes.

$(\sigma_s-\sigma_{so})/\sigma_{so}$ describes the change in σ_s of the PDA coated membranes in comparison to that of the bare one.

A high value of $(\sigma_s-\sigma_{so})/\sigma_{so}$ means that the total surface free energy of the membranes after the PDA coating increases.

Table S4. Surface free energy and its components of the bare membranes.

Membranes	Contact Angle (°)		SFE components (mN/m)		
	Water	Diiodomethane	σ_{so}	σ_{so}^{d}	σ_{so}^{p}
PSF	97.4±0.2	31.6±0.5	43.6	43.5	0.015
PSF-SPES	72.9±0.8	29.8±0.4	49.3	44.3	5.048

σ_{so}: The total surface free energies of the bare membranes.
σ_{so}^{d} and σ_{so}^{p}: Dispersive and polar components of the surface free energies of the bare membranes.

Table S5. XPS analysis of the bare and PDA coated membranes.

Membranes	Coating technique	S%	C%	O%	N%	N/S	C/O
PSF	*	3.86	82.74	13.4	-	-	6.17
	CP	3.00	76.82	16.14	4.04	1.35	4.76
	USP	1.82	74.83	19.11	4.24	2.33	3.92
PSF-SPES	*	7.86	71.12	21.02	-	-	3.38
	CP	4.91	73.61	19.53	1.95	0.40	3.77
	USP	3.73	69.03	21.88	5.36	1.44	3.15

* Bare membrane.

Table S6. Surface roughness of the bare and PDA coated membranes.

Membranes	R_a (nm)	R_q (nm)
PSF	2.53±0.16	3.15±0.19
PSF_CP	5.41±1.45	7.22±2.01
PSF_USP	3.70±0.76	4.67±0.98
PSF-SPES	3.34±0.01	4.26±0.24
PSF-SPES_CP	8.52±3.18	12.01±4.89
PSF-SPES_USP	4.03±0.45	5.23±0.70

Table S7. Influence of PDA deposition on membrane hydraulic resistance.

Membranes	Hydraulic Resistance x 10^{-10} (m^{-1})	
	PSF	PSF-SPES
Bare	415.7	39.4
PDA coated membranes with CP	1547.8	10.7
PDA coated membranes with USP	3549.9	69.1

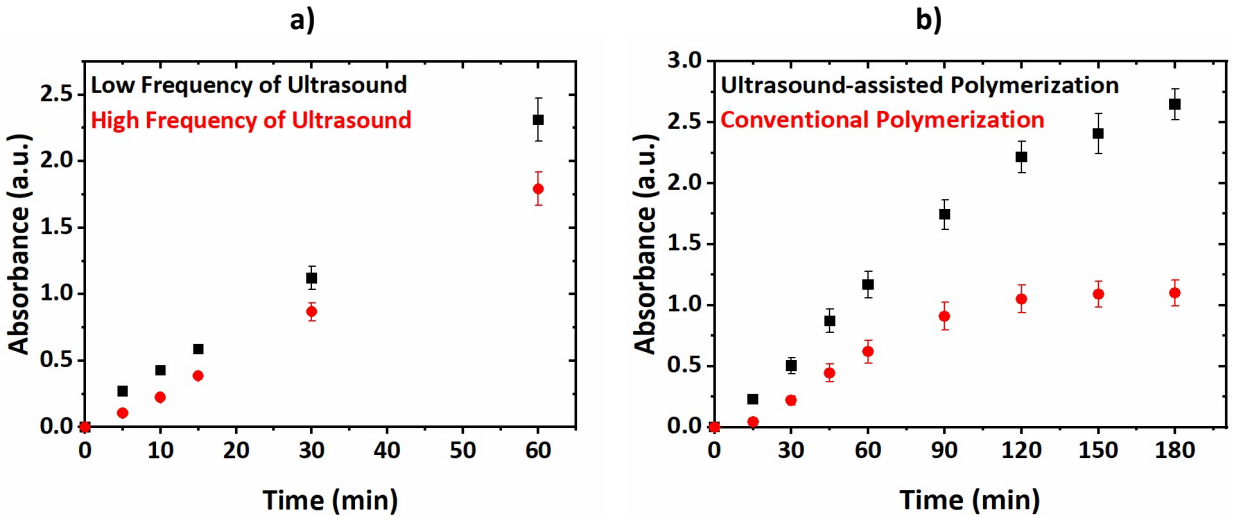

Fig. S1 The rate of dopamine polymerization **a)** Effect of ultrasound frequency on the absorbance of dopamine solution **b)** Absorbance of blue NBT formazan at 560 nm as function of time.

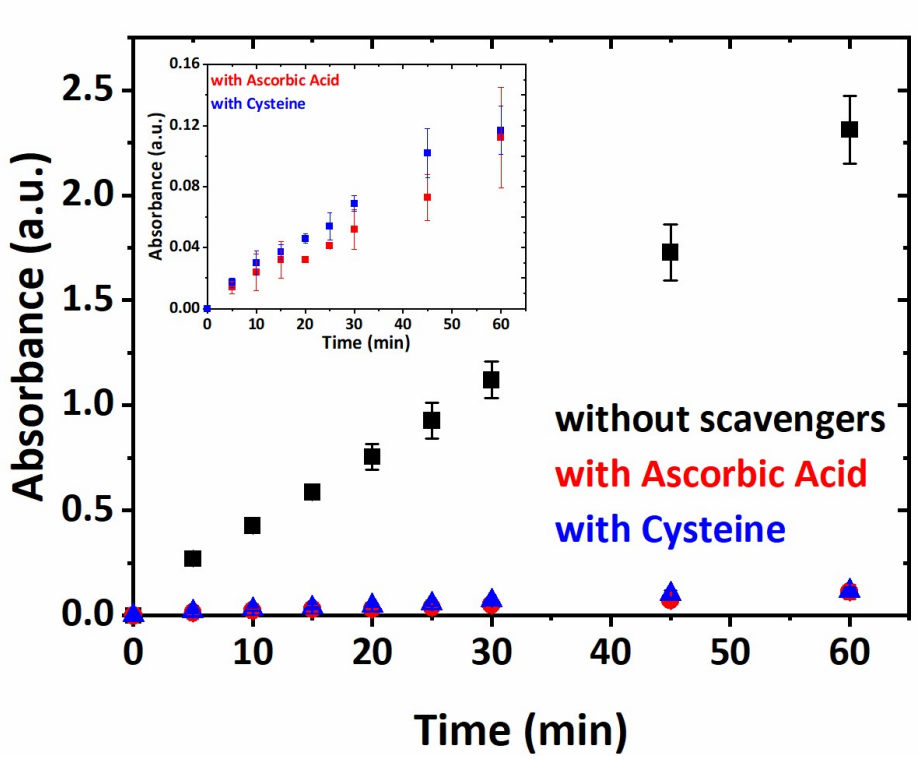

Fig. S2 The effect of scavengers on the absorbance of dopamine solution.

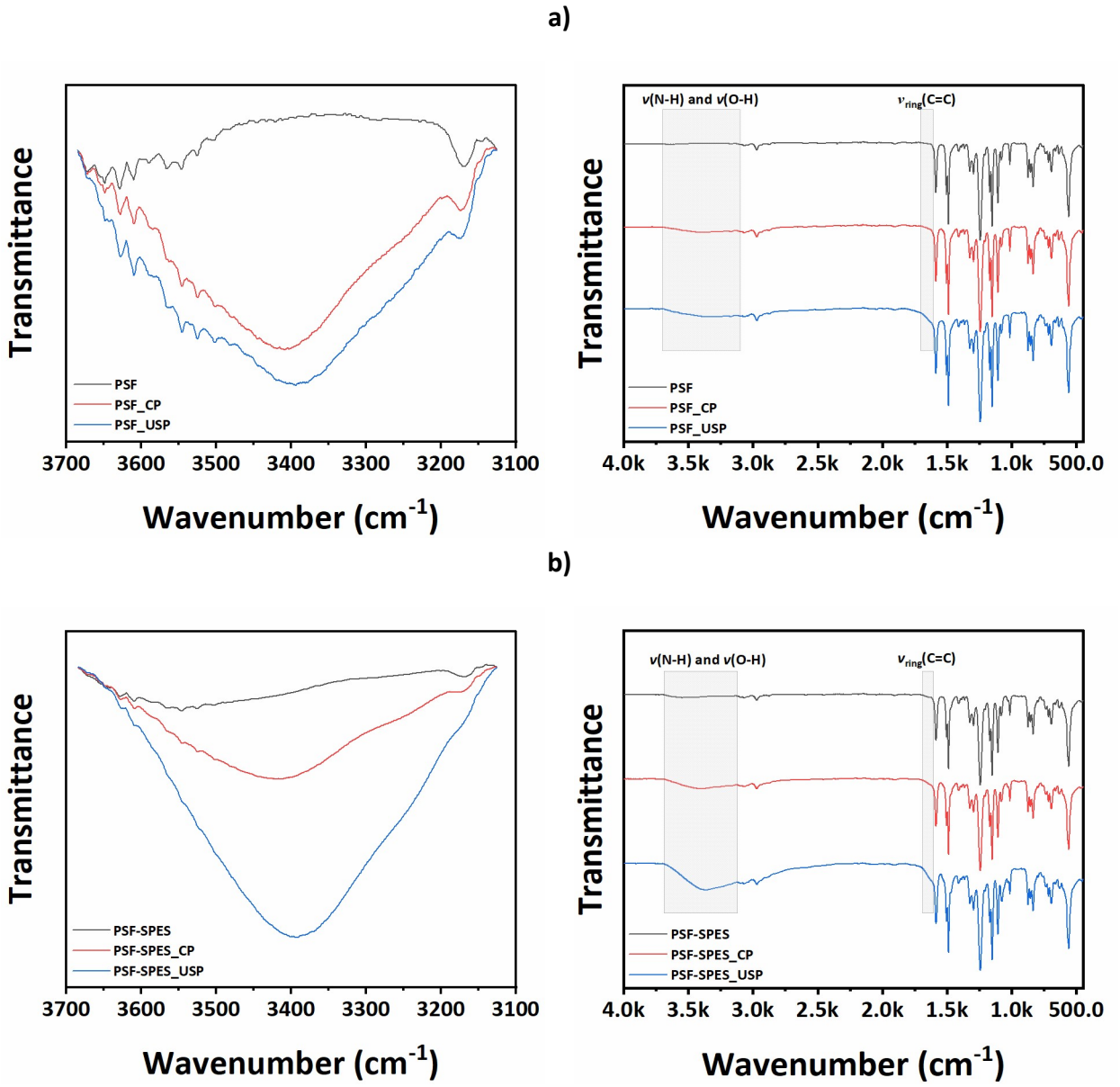

Fig. S3 ATR-FTIR spectra of the bare and modified **a)** PSF and **b)** PSF-SPES membranes.

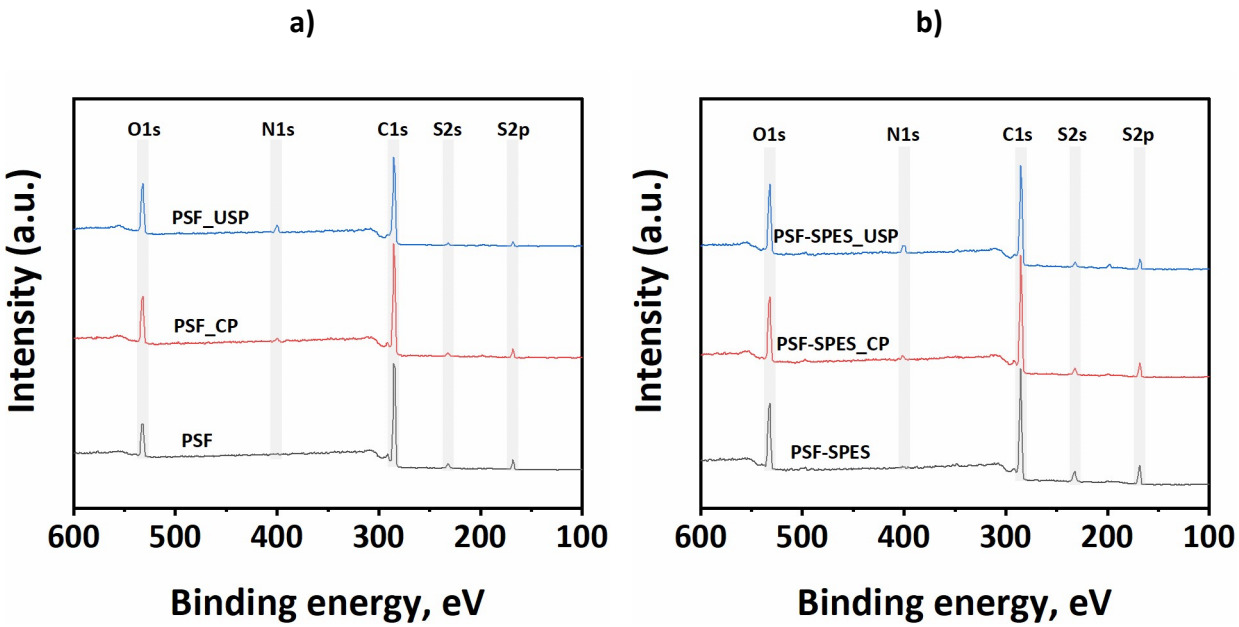

Fig. S4 The general survey of the bare and modified **a)** PSF and **b)** PSF-SPES membranes.

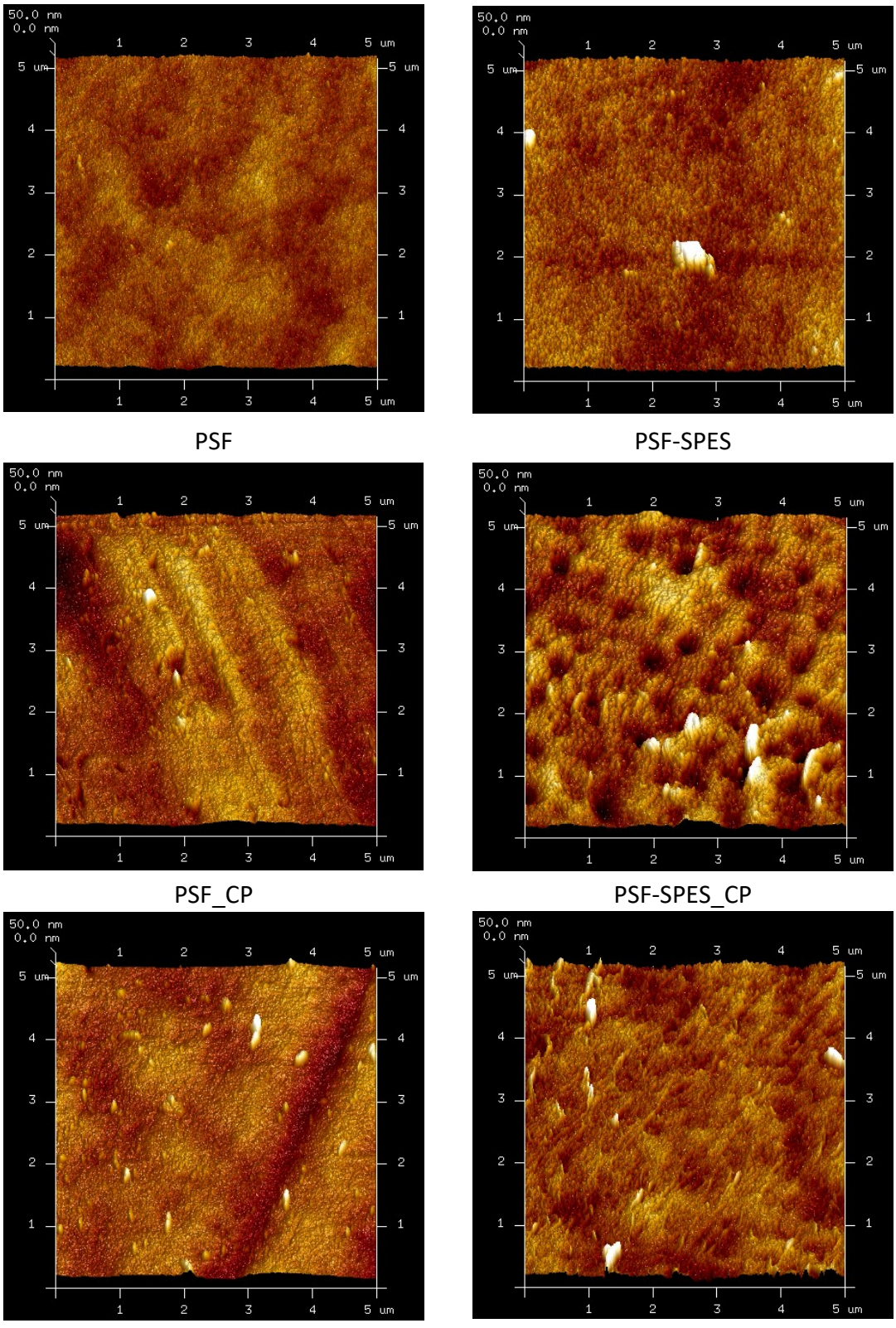

PSF PSF-SPES

PSF_CP PSF-SPES_CP

PSF_USP PSF-SPES_USP

Fig. S5 AFM images of the bare and PDA coated membranes.

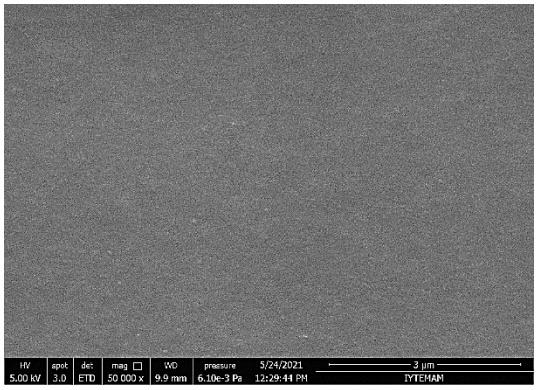

PSF

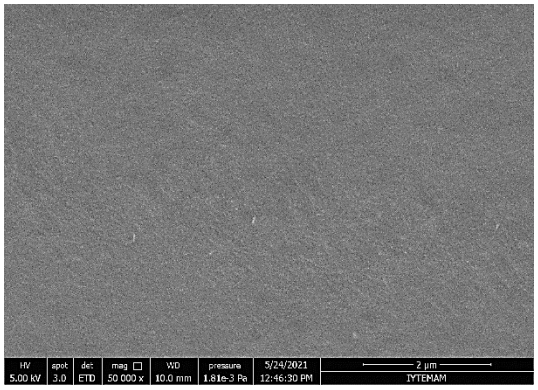

PSF-SPES

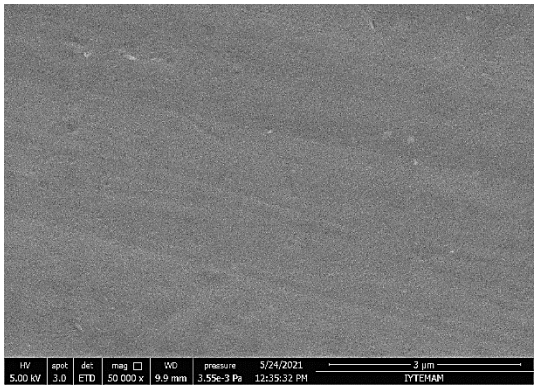

PSF_CP

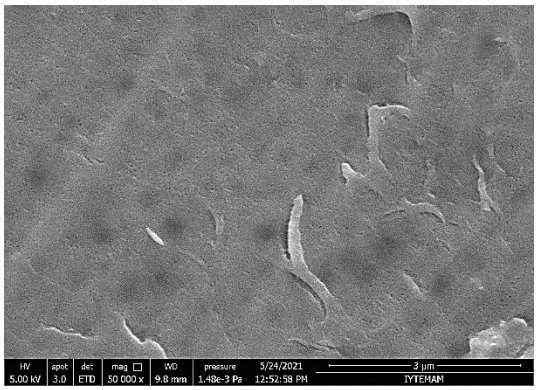

PSF-SPES_CP

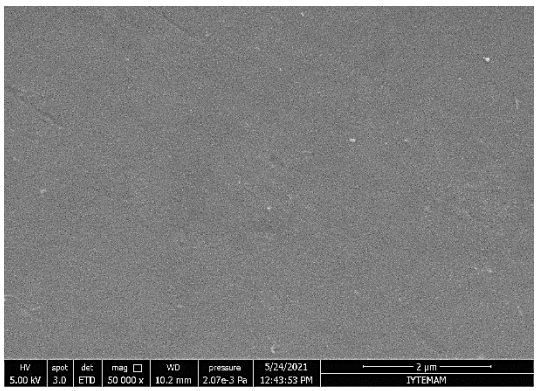

PSF_USP

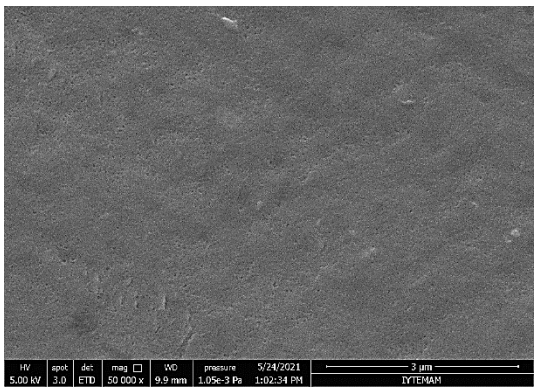

PSF-SPES_USP

Fig. S6 Surface SEM images of the bare and PDA coated membranes.

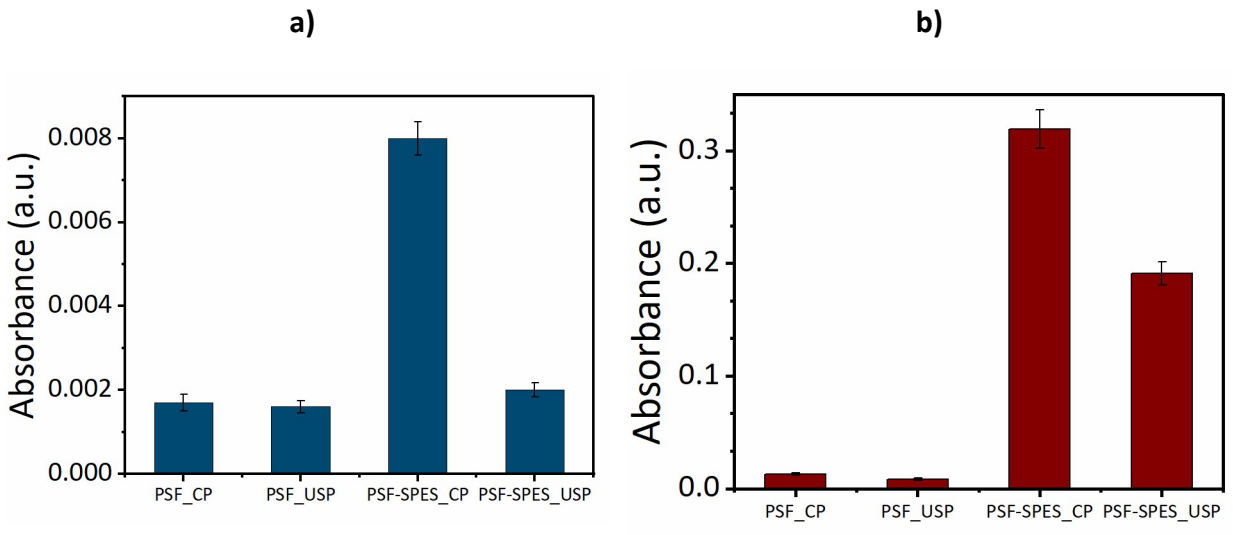

Fig. S7 UV-visible spectra of the eluent of PDA coated membranes immersed in strongly acidic and alkaline solutions: **a)** 0.1 M HCl, **b)** 0.1 M NaOH solutions. The immersion time is 24 h.

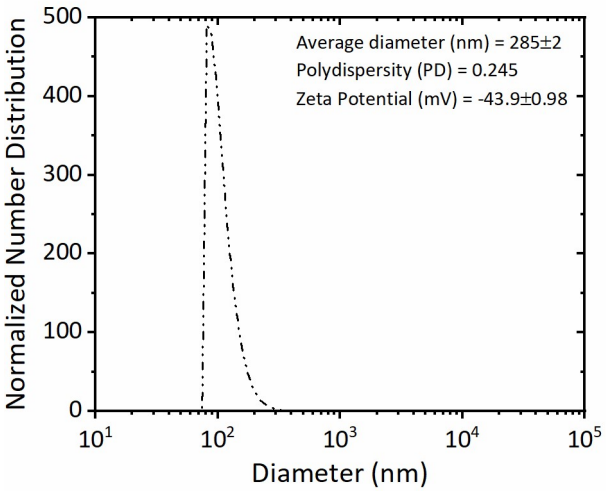

Fig. S8 Size distribution and zeta potential of water/paraffin emulsion used as synthetic foulant in the experiments.

Notes and references

1. J. Jiang, L. Zhu, L. Zhu, B. Zhu and Y. Xu, *Langmuir*, 2011, **27**, 14180-14187.
2. B. D. McCloskey, H. B. Park, H. Ju, B. W. Rowe, D. J. Miller, B. J. Chun, K. Kin and B. D. Freeman, *Polymer*, 2010, **51**, 3472-3485.
3. X. Du, L. Li, J. Li, C. Yang, N. Frenkel, A. Welle, S. Heissler, A. Nefedov, M. Grunze and P. A. Levkin, *Adv. Mater.*, 2014, **26**, 8029-8033.